Mechanical properties of a bio-inspired robotic knifefish with an undulatory propulsor

2011 Bioinspir. Biomim. 6 026004

(http://iopscience.iop.org/1748-3190/6/2/026004)

IOP Publishing Bioinspiration & Biomimetics
Bioinsp. Biomim. **6** (2011) 026004 (9pp) doi:10.1088/1748-3182/6/2/026004

Mechanical properties of a bio-inspired robotic knifefish with an undulatory propulsor

Oscar M Curet[1,4], Neelesh A Patankar[1], George V Lauder[2] and Malcolm A MacIver[1,3,5]

[1] Department of Mechanical Engineering, Northwestern University, Evanston, IL, USA
[2] Department of Organismic and Evolutionary Biology, Harvard University, Cambridge, MA, USA
[3] Department of Biomedical Engineering and Department of Neurobiology and Physiology, Northwestern University, Evanston, IL, USA

E-mail: maciver@northwestern.edu

Received 8 February 2011
Accepted for publication 15 March 2011
Published 7 April 2011
Online at stacks.iop.org/BB/6/026004

Abstract
South American electric knifefish are a leading model system within neurobiology. Recent efforts have focused on understanding their biomechanics and relating this to their neural processing strategies. Knifefish swim by means of an undulatory fin that runs most of the length of their body, affixed to the belly. Propelling themselves with this fin enables them to keep their body relatively straight while swimming, enabling straightforward robotic implementation with a rigid hull. In this study, we examined the basic properties of undulatory swimming through use of a robot that was similar in some key respects to the knifefish. As we varied critical fin kinematic variables such as frequency, amplitude, and wavelength of sinusoidal traveling waves, we measured the force generated by the robot when it swam against a stationary sensor, and its velocity while swimming freely within a flow tunnel system. Our results show that there is an optimal operational region in the fin's kinematic parameter space. The optimal actuation parameters found for the robotic knifefish are similar to previously observed parameters for the black ghost knifefish, *Apteronotus albifrons*. Finally, we used our experimental results to show how the force generated by the robotic fin can be decomposed into thrust and drag terms. Our findings are useful for future bio-inspired underwater vehicles as well as for understanding the mechanics of knifefish swimming.

1. Introduction

Aquatic animal swimmers excel at low-speed motion through complex spaces. Some are particularly adept at this task, and thus warrant study to understand the mechanical principles underlying their behavior. Aquatic animals that are adapted for swimming around coral reefs in marine ecosystems or submerged foliage in freshwater habitats can be informative of novel mechanical principles. This study concerns the robotic emulation of the propulsion mechanism of the weakly electric knifefish from the Amazon Basin, the black ghost (*Apteronotus albifrons*) (figures 1(*A*) and (*B*)). These fish are found hunting at night in root masses along the edges of Amazonian rivers and other areas of dense vegetation. Knifefish use an elongated ribbon-like anal fin as their primary propulsive mechanism. They swim forward by sending undulations along the ribbon fin in the anterior to posterior direction. They can easily swim backward by reversing the direction of the traveling waves, and can move vertically by simultaneously sending traveling waves from the head and tail toward the center of the fin, canceling longitudinal forces and amplifying the vertical force [1]. Combined with other maneuvers, particularly rapid body rolls [2], these capabilities allow them to move omnidirectionally over short time intervals [3].

[4] Present address: School of Engineering, Brown University, Providence, RI, USA.
[5] Author to whom any correspondence should be addressed.

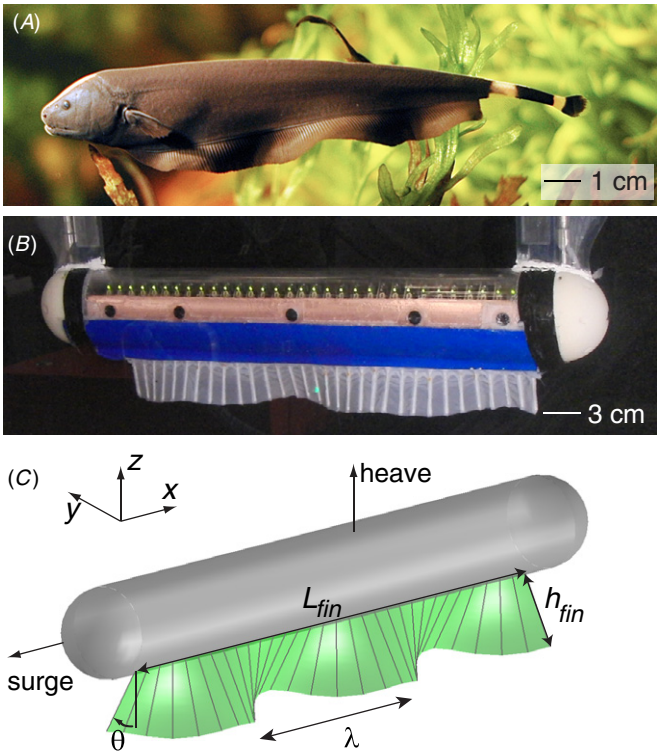

Figure 1. A photograph of the knifefish and its robotic implementation. (*A*) The weakly electric black ghost knifefish, *Apteronotus albifrons*, from South America. Photograph courtesy of Per Erik Sviland. (*B*) The biomimetic robotic knifefish, a physical model to study the principles of undulatory fin propulsion. (*C*) Schematic of the physical model showing the fin length (L_{fin}), the fin height (h_{fin}), the wavelength (λ), the angular fin deflection (θ), the Eulerian reference frame and the robot body frame (*surge* and *heave*).

We would like to understand the basic mechanics of the knifefish fin for ongoing work on relating the biomechanics of the fish to their neuronal processing strategies [4, 5]. In addition, the unique propulsor of this animal is an attractive emulation target since prior work suggests that this mechanism results in multi-directional thrusting that varies smoothly with changes in control parameters [6].

Previous work on knifefish has described their kinematics at different swimming speeds and during different maneuvers [2, 7]. In addition to live animal observations, theoretical models, computational simulations, and bio-mimetic robot studies have provided insight into force generation, flow structure, and the mechanical basis of thrust vectoring [1, 6]. While a number of studies have examined the broader issue of undulatory propulsion in fish [6–14], few [10] address the relationship between force generation, swimming velocity, and key undulatory parameters.

In this study, we seek to fill this gap in our understanding by examining how propulsion capability changes as basic fin actuation properties are systematically varied. We used a biomimetic robot knifefish model (see figure 1(*B*)) for this purpose. Previous work with such physical models of fish has contributed significantly to our knowledge of how they generate propulsive forces [15–21]. In this work, we model the fish's fin motion with a sinusoid, and we study how the force from the robot varies with wave amplitude, frequency, and wavelength. We also examine how swimming velocity varies with these key fin actuation properties. From these results, we have found that there is an optimal operational region in the fin's actuation parameter space.

In addition to the measurements of force and velocity, we measured the drag of the robot at different flow speeds, as well as the fin drag at different flow speeds and configurations. With these experimental measurements we are able to separate the contributions of drag and thrust during undulatory swimming.

2. Materials and methods

2.1. The robotic knifefish

All experiments were carried out with a robotic knifefish designed in collaboration with Kinea Design LLC (Evanston, IL, USA). The basic shape and capabilities of the robot were based on the black ghost knifefish *A. albifrons*. The robotic fin is 32.60 cm long (L_{fin}) and 3.37 cm high (h_{fin}), as shown in figure 2 (see figure 1(*C*) for the definition of these parameters). These dimensions preserve the $h_{\text{fin}}/L_{\text{fin}} = 0.1$ proportions present for the 1 cm high and 10 cm long fin of a typical adult *A. albifrons*. The mass of the robot is 2.3 kg, and it is neutrally buoyant.

In order to meet our need for a high number of independently controlled fin rays, a stackable 'fish steak' actuator design was developed (figure 2(*B*)). Each fish steak consists of a custom printed circuit board containing ICs for communication and motor control, and a stack-through connector along the top edge of each module formed a signal and power bus, while also providing mechanical support to the assembly. Connected together, the fish steaks formed an integral part of the mechanical structure of the robot body for attachment of the fin ray control motors. Thirty-two 10 mm motors (RE10, Maxon Motor AG, Sachsein, Switzerland), with 64:1 gear reducers and encoders, were arranged in a spiral overlapping arrangement to minimize the length of the robot. The rated torque for each fin ray was 50 mN m.

For communication, a controller area network (CAN) bus was used, with signals generated through a real-time kernel (xPC Target, MathWorks, Natick, MA, USA) running on a PC104 stack running outside of the robot. Power and control signals were sent via a multichannel tether.

For the fin, stainless steel (316 Stainless) was turned down to 1.4 mm at the base tapering to 0.89 mm at the tip for the 32 rays, and a custom double-layer lycra fin was attached. Spacing between the fin rays was 1 cm. The Young's modulus of this fin material is approximately 0.2 MPa, similar to that of fish inter-ray membrane [22].

2.2. Swimming velocity measurements

The schematic of the experimental setup to measure the swimming velocity of the robotic knifefish is shown in figure 3(*A*). To obtain the robot swimming velocity, we used a technique previously detailed by Lauder *et al* [19]. In this technique, the robot was suspended from a low friction air bearing (S301301, New Way Air Bearings, Aston, PA, USA).

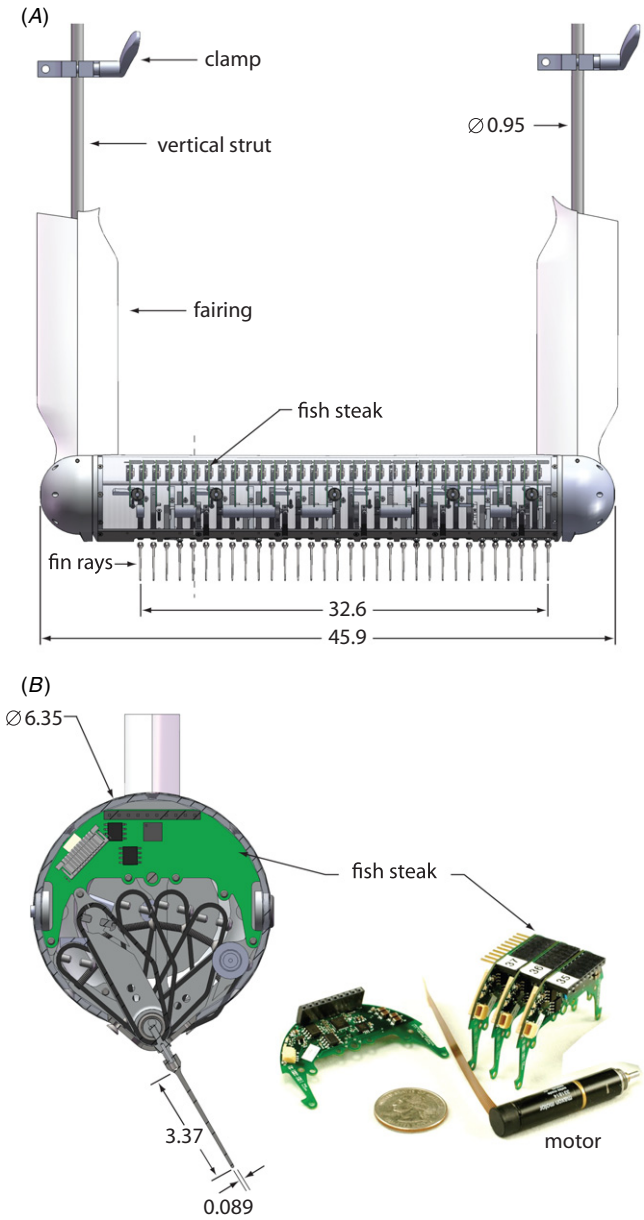

Figure 2. Robotic knifefish design and dimensions (all dimensions in centimeters). (*A*) Side view. The body of the robot is a cylinder with hemispherical end caps at both ends. The body is suspended from frictionless air rails using the two vertical struts shown through attachment to a mounting platform. Fairings are used to reduce the drag of the vertical struts. Each fin ray is controlled by an independent motor and 'fish steak'. (*B*) Cross-section of the robot and photograph of the stacking fish steaks used for motor control.

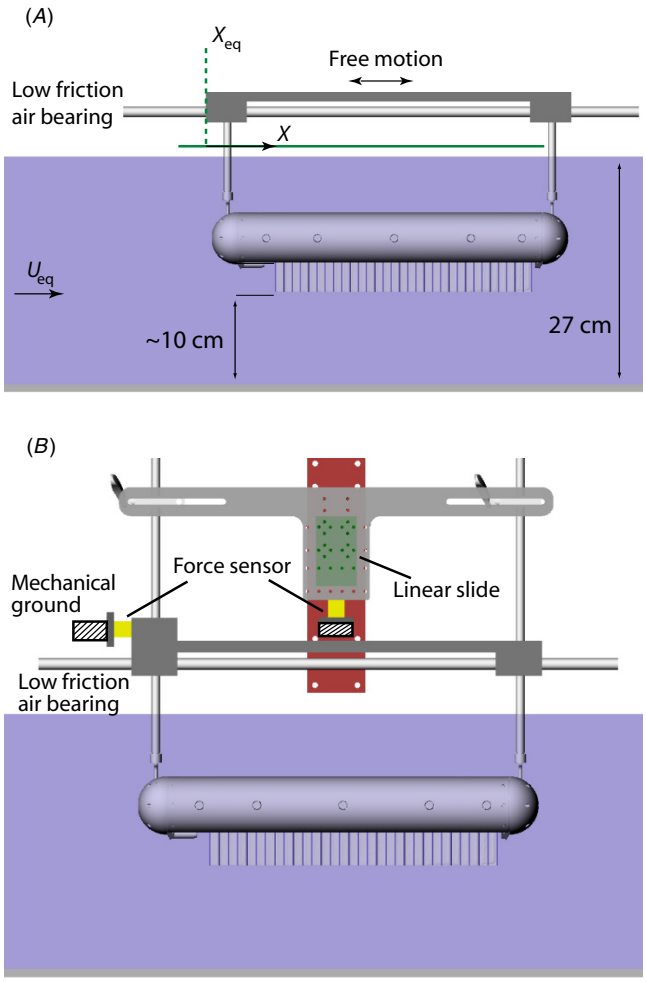

Figure 3. Schematics of the experimental setups for velocity and force measurements. (*A*) Measurement of free swimming velocity. The robot was suspended from a low friction air bearing system that allowed free forward and backward motion. After the ribbon fin was activated, the speed of the flow tank was adjusted until the robot reached its initial equilibrium point, X_{eq}. (*B*) Measurement of the surge, heave and drag forces. The robot was suspended from a low friction air bearing that allowed forward and backward motion, and a high precision mechanical slide that allowed vertical motion. Two one-dimensional force sensors were used to measure the forces generated in the longitudinal and vertical directions.

In still water and with no fin actuation, the robot reaches an equilibrium point, X_{eq}. Once the fin is actuated and the robot starts swimming, the speed of the flow tank is adjusted until the robot reaches the initial equilibrium point X_{eq}. The flow speed when the robot stabilizes to the initial equilibrium point is equal to the robot swimming speed, U.

Following this technique, we performed three sets of experiments to obtain the robot swimming velocity as a function of the fin actuation parameters, frequency (f), number of waves (# waves), and maximal angular deflection (θ) of the fin rays. The number of waves is defined as L_{fin}/λ, where λ is the wavelength. The angular deflection of the fin is measured from the robot midsagittal plane. For each set of experiments, one parameter was changed, while the other two parameters were held constant. The fin parameters to measure the robot swimming velocity correspond to set 1, set 2, and set 3 from table 1. Velocity and force measurements were performed in a water flow tank with a working volume of 80 cm × 28 cm × 27 cm in length, width, and depth, respectively.

To estimate the error in our measurements of swimming velocity, we performed an additional set of experiments. The swimming velocity was measured in five consecutive trials with identical motion parameters for the fin (f = 3 Hz, # waves = 2 and $\theta = 30^{\circ}$). Between each trial the flow tank was turned off. At the beginning of each trial, the speed of the flow was equal to zero.

Table 1. Fin actuation parameters for velocity and force measurements.

Experimental set	f (Hz)	# waves (L_{fin}/λ)	θ (deg)
Set 1	0.5, 1.0, 2.0, 3.0, 4.0, 5.0, 6.0	2	30
Set 2	4.0	0.5, 0.8, 1.0, 1.5, 2.0, 2.2, 2.5, 2.8, 3.0, 4.0	30
Set 3	4.0	2	10, 20, 25, 30, 35
Set 4 (force measurements only)	2.0, 3.0, 4.0, 5.0	2	35

2.3. Force measurements

Forces generated by the robotic knifefish. Figure 3(*B*) depicts a schematic of the experimental setup to measure the forces generated by the robotic knifefish. The robot was suspended from low friction air bearings which allow motion along the longitudinal axis. The robot was also mounted on a linear slide to allow vertical motion (Parker Automation, Irwin, PA, USA; model 4201). This experimental setup allowed measurement of forces in both of these directions. Following standard nomenclature, we refer to the force along the longitudinal axis as the surge force, and the force in the vertical direction as the heave force. The surge force was measured with a 44.5 N-capacity force sensor (Futek Advanced Sensor Technology, Irvine, CA, USA; model LSB200, 10 lb). The heave force was measured with a 9 N-capacity force sensor (Futek Advanced Sensor Technology, Irvine, CA, USA; model LSB200, 2 lb). The force signals were acquired at a sample rate of 400 Hz with the Chart data acquisition system (ADInstruments, Colorado Springs, CO, USA). All forces measurements were acquired long after the initial transient period had passed.

Similar to the swimming velocity measurements, forces were measured as a function of frequency, number of waves, and maximal angular deflection. The parameters for each of the experimental sets are shown in table 1. For experimental sets 1, 2 and 3, only surge force was recorded. For experimental set 4, surge and heave force were recorded simultaneously.

To estimate the error in our force measurements we performed an additional set of experiments. The surge force was measured in five consecutive trials with identical parameters. For those trials, the fin was actuated with $f = 3$ Hz, # waves $= 2$ and $\theta = 30^\circ$.

Drag measurements. Across a set of flow speeds, we measured the drag of the fish robot with the fin straight, and after raising the robot so that only the fin was in the water to measure the drag of the fin alone. In addition, we measured the drag of the fin at different angles of deflection at a single flow speed. The experimental setup for the drag measurements was the same as the experimental setup for the force measurements described above.

For the robot drag measurement, the fin was held straight ($\theta = 0^\circ$) and the speed of the flow tank was varied from 4.5 to 38.5 cm s^{-1}. To measure the drag of the fin at different flow speeds, the fin at $\theta = 0^\circ$ was submerged into the flow tank. In another set of measurements, the fin drag was measured as a function of angular deflection. For these measurements, only the fin was submerged and the flow speed was constant at 18 cm s^{-1}. The fin had two full waves along the fin length, and the maximum angular deflection, θ, was varied from 10 to 35°. The fin was held stationary in this position (the undulation frequency was 0 Hz). To estimate the error of the drag force measurements, the force data was subdivided into three time intervals of 20 seconds each. From these time intervals, we computed an average force. The error was estimated from the maximum and minimum force average.

3. Results

The robotic knifefish swimming velocity, U, as a function of the fin actuation parameters (frequency, number of waves and angular deflection) is shown in figures 4(*A*)–(*C*). To show how the frequency and number of waves affect the swimming velocity relative to the velocity of the traveling wave along the fin, we plot the swimming velocity normalized by the wave speed in the bottom graphs of panels *A* and *B*. The wave speed is defined as $V_{\text{wave}} = f\lambda$, where f is the frequency and λ is the wavelength. V_{wave} is constant with variation of maximum angular deflection. For the case where only maximal angular deflection was varied (figure 4(*C*)), we normalized the swimming speed with the average lateral speed of the fish V_{lateral}. V_{lateral} is defined as $V_{\text{lateral}} = 4df$, where $d = h_{\text{fin}} \sin(\theta)$. Note that in one wave cycle, a transverse section of the fin travels four times the distance d.

From figure 4(*A*) we can observe that the swimming speed increases as the frequency increases. However, there is a peak in the swimming speed relative to the wave speed (U/V_{wave}) at $f = 1.0$ (figure 4(*A*), bottom). Then, for larger frequencies, U/V_{wave} decays. For swimming velocity as a function of the number of waves, figure 4(*B*), the swimming velocity first increases with the number of waves until it peaks at around two waves on the ribbon fin. As the number of waves is further increased, the swimming velocity starts to decrease. In the last case, figure 4(*C*), the swimming speed increases with the amplitude of oscillation.

Figure 5 shows the surge force generated by the robotic knifefish as a function of fin frequency, number of waves and angular deflection. The surge force increases exponentially as a function of frequency (figure 5(*A*)). On the other hand, the surge force increases with the number of waves and peaks around two full waves on the ribbon fin. For a higher number of waves, the surge force declines (figure 5(*B*)). As can be observed in figure 5(*C*), the surge force increases as we increase the amplitude of oscillation on the ribbon fin. In figure 5, our estimates based on the previous simulation of an undulating fin [6] and the estimates of Lighthill and Blake [11] are also shown. Note that the estimates of [6] are based on simulations for a fin with dimensions similar to *A. albifrons* (1 cm tall and 10 cm long), that have been scaled by the height and length of the robot fin (3.37 and 33 cm, respectively).

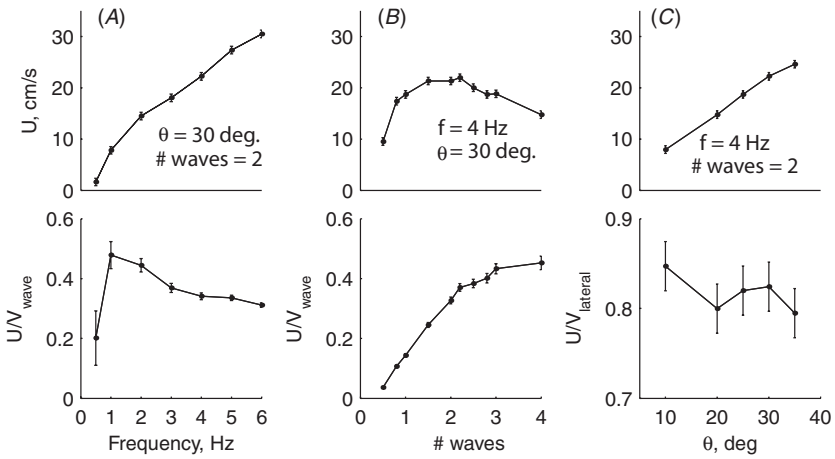

Figure 4. Robotic knifefish swimming velocity as a function of frequency (*A*), number of waves (*B*), and angular deflection (*C*). In the bottom graphs, the swimming velocity is normalized by the respective velocity scale, wave speed for (*A*) and (*B*), and lateral velocity for (*C*). The standard deviation of the error is shown with error bars.

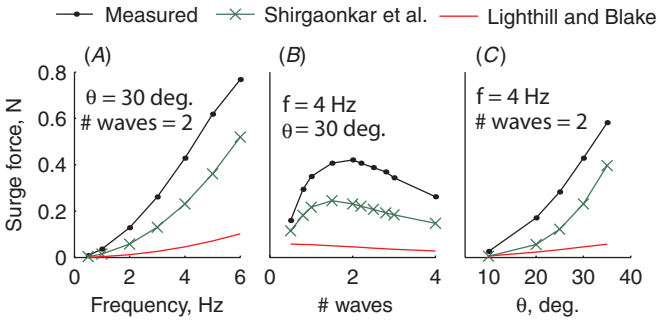

Figure 5. Robotic propulsive force as a function of frequency (*A*), number of waves (*B*), and angular deflection (*C*). Also shown are our previous estimates (Shirgaonkar *et al* [6]) based on a smaller ribbon fin, and the Lighthill and Blake estimates [11]. The standard deviation of the error on the force measurements is less than 1.5% (the error bars will not appear at this scale).

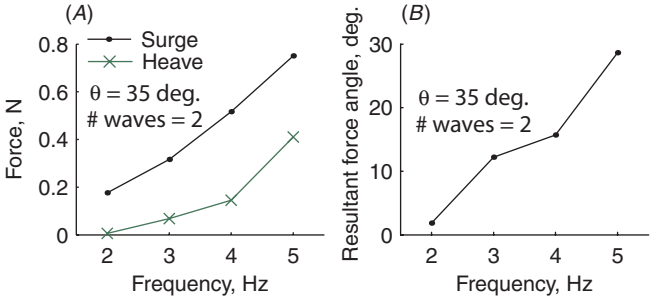

Figure 6. Robotic forces and resultant force angle. (*A*) Robotic surge and heave forces as a function of frequency. (*B*) Resultant force angle as a function of frequency. The standard deviation of the error on the force measurements is less than 1.5 % (the error bars will not appear at this scale).

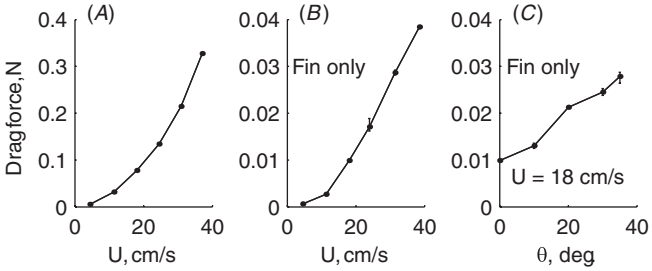

Figure 7. Drag measurements. (*A*) Robotic knifefish drag as a function of flow speed. The fin was held straight. (*B*) Fin drag as a function of flow speed. The fin was held straight. (*C*) Fin drag as a function of maximal angular deflection for a flow speed of 18 cm s^{-1}.

Significant differences can be expected given the much larger fin size of the robot. Despite this issue, the qualitative trends in experimental and computed force are similar. In contrast, the qualitative trends from Lighthill's theory do not agree well with experimental results. The primary mechanism of thrust production in ribbon fins is an axial jet along the lower edge of the ribbon fin [6]. Lighthill's theory does not capture this mechanism of thrust production.

Figure 6(*A*) shows the variation of surge and heave force as a function of frequency. Figure 6(*B*) depicts how the resultant force angle changes for different frequencies. The resultant force angle is equal to $\tan^{-1}(F_{\text{heave}}/F_{\text{surge}})$, where F_{heave} and F_{surge} are the heave and surge forces, respectively. The surge and heave forces increase with frequency. The resultant force angle also increases with an increase in the traveling wave frequency.

The drag of the robotic fish with the fin straight is shown in figure 7(*A*). Figures 7(*B*) and (*C*) depict the drag of only the fin of the robot as a function of flow speed and as a function of angular deflection, respectively.

4. Discussion

4.1. Swimming velocity

In a previous study by Blake [7], it was suggested that the main parameter to control cruising speed for the knifefish is the fin oscillation frequency. Blake showed this to be the case in a different kind of fish that uses elongated midline fins at the top and bottom edge of the body, termed balistiform swimming, such as found in triggerfish [10]. Similar to

Blake's observation on balistiform swimmers [10], our results suggest that there is a minimum non-zero frequency that needs to be reached to start swimming (see figure 4(*A*)). In our robotic knifefish, the minimum frequency is around 0.4 Hz. We propose that this minimum frequency needed to start swimming is related to the drag generated by the undulatory fin and robot body. As we will discuss in greater detail below, the net force generated by the undulatory ribbon fin can be decomposed into the thrust and drag of the fin. If the thrust that the undulating fin generates is not large enough to overcome the sum of the drag of the fin itself and the body drag, then the robot or fish will not swim [23]. For large frequencies (greater than 2 Hz in our robotic system), the swimming velocity changes almost linearly with frequency. These results are consistent with Blake's observations of balistiform swimmers [10].

The bottom graph of figure 4(*A*) shows the variation of the swimming speed normalized by the wave speed (U/V_{wave}) as a function of frequency. U/V_{wave} is also referred to as the wave efficiency [24, 25] or slip [26]. This quantity is equivalent to comparing how far the swimmer has traveled to how far the undulatory wave has traveled in a given time period. Based on the wave efficiency, the best performance of the fin occurs at low frequencies of around 1 Hz. For high frequencies, the wave efficiency slowly decays. This result agrees with prior conjectures that undulatory fin propulsion in knifefish is mechanically efficient for slow speeds [7]. For a knifefish that hunts slow-swimming prey in a complex environment, there is no need to have a highly efficient propulsion system for high velocities, but instead one that can provide high maneuverability and efficiency at slow to moderate swimming velocities. Even though the wave efficiency is better at low frequency, the maximum swimming speed increases for the range of frequency tested. This is important in situations such as prey capture, where the maximum speed is desired over the efficiency.

We found that the wave efficiency peaked at approximately 0.5. However, for *A. albifrons* the wave efficiency is between 0.6 and 0.9 [27] and for the American eel, *Anguilla rostrata*, approximately 0.8 [26]. A possible reason for the difference between the wave efficiency of the robot and the knifefish is that the body of the fish is more streamlined than the robot, resulting in a higher drag coefficient for the robot. The drag coefficient for knifefish is approximately 0.24, using drag force data for a urethane cast of *A. albifrons* from [4], and a frontal area of 3.62 cm^2. The drag coefficient of the robot based on frontal area is around 1.5 for high Reynolds numbers (see figure 8). Note that we could not measure the input power to drive the motors during our experiments. Therefore, we can only benchmark the performance of the robot through a comparison of the swimming velocity to the wave velocity or the lateral velocity. However, this comparison does not take into account hydrodynamics or elastic forces to actuate the fin. Also note that the peak performance could change depending on the wave amplitude and number of waves. Knifefish tend to actuate their fins in one of two ways: (1) low frequency, low number of waves, and high amplitude or (2) high frequency, high number of waves, and small amplitude [7]. Our tests are restricted to the first type of fin actuation.

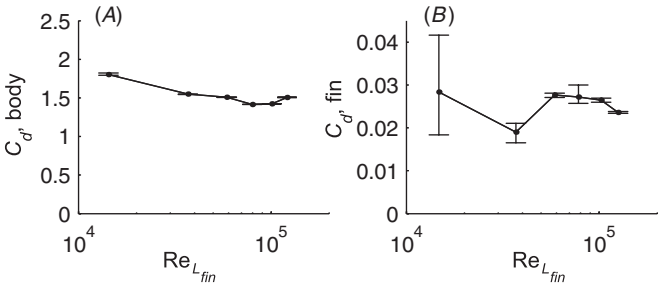

Figure 8. Drag coefficients for the robotic knifefish body (*A*), and for the straight fin (*B*). The Reynolds number is based on the length of the ribbon fin, L_{fin}.

The top graph of figure 4(*B*) shows that the swimming velocity peaks when there are around two waves along the fin. This is also consistent with the peak force that the fin can generate for a given frequency and maximum amplitude (see figure 5(*B*)). This is an interesting result that was predicted in our previous computational simulations [6]. It has been previously [7] reported that during forward swimming knifefish have between 2.5 (in electric knifefish) and 1.7 waves on the fin, depending on the fish family. In our previous study [6], we hypothesized that the peak in force production at around two waves along the fin results from the interaction of two competing effects: (1) an increase in the wetted surface area that can produce greater force on the fin as the number of waves increases, and (2) a decrease of wave speed that produces weaker force on the fin as the number of waves increases.

The bottom graph of figure 4(*B*) illustrates how U/V_{wave} initially increases as the number of waves increases and then levels off. The rate of change of U/V_{wave} decreases significantly above two waves on the ribbon fin. Also above two full waves, the swimming speed starts to decrease (figure 4(*B*), top). Thus, based on pure kinematics, the best performance occurs between two and three waves where U/V_{wave} starts to plateau and the swimming velocity is considerably higher than for four waves. However, this does not take into account the elastic or hydrodynamics forces. For example, for a given fin length and number of rays (32 for the robotic fish, and more than 100 for *A. albifrons*), as the number of waves increases, so does the phase difference between rays. The larger phase difference implies an increase in the force to stretch the fin material between the rays. Therefore, it is possible that an optimal operational point with respect to the wavelength (at constant amplitude and frequency) differs from the point of the maximum wave efficiency.

As can be observed from the top graph of figure 4(*C*), the swimming velocity varies linearly with the maximum angle of deflection. The bottom graph of that panel shows how the swimming velocity normalized by the lateral velocity, U/V_{lateral}, changes with amplitude. The variation of U/V_{lateral} is only from 0.85 to 0.78, and the highest kinematic performance is at $\theta = 10^\circ$ for the specified frequency and number of waves. The fin performance also has a local maximum between $\theta = 25$ and 30°. *A. albifrons* swims with an angular deflection similar to 30° at higher swimming

velocities [27]. However, other types of knifefish swim with lower angular deflection at higher frequency. The operational point may be a tradeoff between the optimal frequency and the angular deflection at a given swimming speed.

4.2. Force

Figure 5 shows the surge force generated by the robotic knifefish as a function of frequency, number of waves and angular deflection. The figure also shows our estimates based on a scaling relationship obtained from simulations of a ribbon fin of $L_{\text{fin}} = 10$ cm and $h_{\text{fin}} = 1$ cm, approximately the size of the anal fin of an adult *A. albifrons*. The estimates of Lighthill and Blake [11] are also shown. As discussed before, the estimates by Lighthill and Blake do not agree even qualitatively with the experimental data because their theory does not capture the primary mechanism of thrust production [6]. Although the magnitude of our previous force estimate underestimates the measured force by a factor of 1.7, all the trends of the surge force are qualitatively consistent. A possible reason for the discrepancy between the simulations and the measured force is the large difference in the Reynolds numbers (Re, the ratio of inertial to viscous forces) in the two cases. Here, based on the fin length (L_{fin}) and the wave speed (V_{wave}), for the robot we have $Re \sim 1.5 \times 10^5$, while for the fish it is an order of magnitude lower, at $Re \sim 1.5 \times 10^4$. In addition, the simulations did not model the compliance of the fin ray material.

Figure 6(A) depicts the results for experimental set 4 from table 1 where the surge and heave forces generated by the robotic knifefish were recorded simultaneously. In this case, the frequency of the fin was varied from 2 to 5 Hz while the number of waves and the maximum deflection were kept constant at 2 and 35°, respectively. As expected, the surge force is dominant but the heave force is not insignificant. The contribution of heave increases with frequency. Figure 6(B) shows the resultant force angle generated by surge and heave. The resultant angle increases with frequency, with a range of 2–30°. The angle for a frequency of 3–4 Hz is around 12–15°. This resultant angle is comparable with the angle of insertion of the ribbon fin in various types of knifefish [28]. The angle of insertion of the fin is the angle that the base of the ribbon fin makes with the longitudinal axis (i.e. the axis that goes from the nose to the tail of the fish). During cruising, when the body is held at neural pitch (0°), the 12–15° insertion angle of the fin therefore maximises the thrust that the fish can obtain from the fin.

4.3. Drag

In our last set of experiments we measured the drag of the body and ribbon fin. Figure 7(A) shows the drag measurements of the robot knifefish with the ribbon fin straight versus flow speed. Figure 7(B) depicts the drag of only the straight fin. Figure 8 shows the drag coefficient, C_d, of the robot body and the ribbon fin when it is straight. $C_d = F_{\text{drag}}/(0.5\rho U^2 A)$, where F_{drag} is the drag force, ρ is the water density, U is the swimming velocity and A is the characteristic area. The C_d of the body is obtained after subtracting the drag of the ribbon fin. A is the frontal area of the robot body. For the C_d of the fin, $A = L_{\text{fin}} h_{\text{fin}}$. The drag coefficient of the robot body is indicative of a laminar flow regime where inertial effects are increasingly dominant [29]. This is apparent from the flattening of the drag coefficient at larger Reynolds numbers. However, the fluid flow seems to be transitioning from laminar to turbulent flow around the straight fin after $Re >\sim 4 \times 10^4$. This is evident from the sharp rise in the drag coefficient that is typical of the transition from laminar to turbulent flow over a flat plate [29]. In addition, free surface effects could contribute to the sharp rise in the fin drag coefficient. The Reynolds number was calculated based on the fin length, L_{fin}, and the flow speed. For the experiments where only the angular deflection was varied, the drag force scaled with the angular deflection.

4.4. Thrust and drag generated by the undulatory fin

Decomposing the thrust and drag generated by an undulatory fin or anguilliform swimmer is challenging because the fin is simultaneously generating thrust and drag along its length. Despite this, Patankar *et al* have recently discovered a method to decompose thrust and drag for undulatory swimmers [23]. Here we use our experimental data to test the validity of this result, which was based on computational fluid dynamics.

For this analysis, we consider the net force generated by the undulatory ribbon fin of the robotic knifefish as a function of the frequency of the traveling wave, f. Consider an undulatory ribbon fin with a traveling wave speed, V_{wave}, and swimming velocity, U. The angular deflection, θ, and the wavelength, λ, are held constant. In this case, according to [23], the net force generated by the fin can be expressed as

$$F[U, V_{\text{wave}}] = T[V_{\text{wave}} - U] - D_f[V_{\text{wave}}], \tag{1}$$

where F is the net force generated by the fin, T is the thrust generated, and D_f is the drag of the fin. The square brackets represent 'function of'. Thus, F is a function of U and V_{wave}. For the thrust and drag term, we assumed the following expression:

$$T[V_{\text{wave}} - U] = a_1 (V_{\text{wave}} - U)^2, \tag{2}$$

$$D_f[V_{\text{wave}}] = b_1 V_{\text{wave}}^{b_2}, \tag{3}$$

where a_1, b_1, and b_2 are constants. From our experimental results we found that $a_1 = 1.22$, $b_1 = 0.39$, and $b_2 = 2.80$. To obtain these values, we considered the force, F_o, generated by the robot when it was stationary and the force, F_{fs}, generated by the robot when it was swimming. When the robot knifefish is swimming at steady state, the net force generated by the fin, F_{fs}, must be equal to the drag of the robot body. Thus, F_{fs} was obtained from the drag measurements of the robotic fish body (figure 7(A)) after subtracting the drag of the straight fin (figure 7(B)). F_o is the force measured when the robot is stationary (figure 5(A)). a_1 was obtained from equation (1) after subtracting the expressions for F_{fs} and F_o. Thus, $a_1 = (F_{fs} - F_o)/(U^2 - 2U V_{\text{wave}})$. Once a_1 is known, we can estimate the drag on the fin solving for D_f in equation (1), using the force generated by the robot when swimming, F_{fs}. Thus, D_f *estimated* $= a_1 (V_{\text{wave}} - U)^2 - F_{fs}$. Figure 9 shows

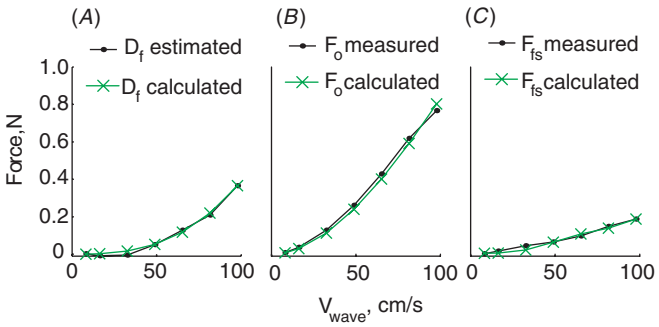

Figure 9. Thrust and drag generated by the undulatory fin compared with our model of thrust and drag decomposition. (*A*) Drag generated by the undulatory fin. (*B*) Net force generated by the undulatory fin when the swimming velocity is zero. (*C*) Net force generated by the undulatory fin when the fin is swimming.

thrust and drag generated by the undulatory fin compared with our model of thrust and drag decomposition. The agreement is excellent. For equations (2) and (3), the effect of the Reynolds number is taken into account with V_{wave}, and a_1. The quadratic dependence of force on velocity indicates that force generation is dominated by inertial effects.

Note that b_1 and b_2 were obtained from data fitting for the drag of D_f *estimated* (see figure 9(*A*)) taking into account only the four highest V_{wave} values. For a_1 we did not consider the lowest V_{wave} velocity.

In previous work, Lighthill and Blake [11] derived an equation to calculate the propulsive force, F_{fs}, generated by an undulating ribbon fin attached to a body. The body was represented as a flat plate. Using the equation they derived, the propulsive force of the robotic knifefish is 0.022 N, with $f = 3$ Hz, $\theta = 30^\circ$, two full waves along the fin length, and swimming at a speed 18 cm s^{-1}. This calculated propulsive force is around three times lower than the propulsive force that the robotic knifefish generates (∼0.067 N) under those conditions. Even though Lighthill and Blake's equation predicted the drag force of different types of knifefish [7], it underestimates the propulsive force that the robotic knifefish generates. As we have discussed previously in [6], Lighthill and Blakes's force analysis does not include hydrodynamic interactions that occur lengthwise along the ribbon fin. Instead, the flow is approximated as two-dimensional flow and assumed to be inviscid.

5. Conclusion

Unveiling the mechanical basis of the agility of swimmers is a complex task that requires a multidisciplinary approach spanning live animal observation, computational, theoretical, and robotic studies. In this work, we focused on understanding the role of key actuation parameters on ribbon fin-based propulsion, a mechanism used by a large group of agile swimmers, including the black ghost knifefish (*A. albifrons*). Toward that goal, we developed a robotic knifefish which allowed us to systematically change the fin actuation parameters. Using this robot, we measured surge and heave forces, and swimming speeds as a function of fin frequency, amplitude and number of waves. Our results shows that there is an optimal operation region for each of these parameters. In addition, we were able to show how the force generated by the robotic fin can be decomposed into thrust and drag. These findings have the potential to facilitate the design, control and development of future autonomous underwater vehicles propelled using undulatory fins. In addition, they will facilitate our understanding of the mechanical properties of weakly electric fish, for which sensing and movement are closely linked due to the short range of active electrosense [3].

Acknowledgments

The authors thank Michael Peshkin, Julio J Santos-Munné, Traveler Hauptman, and Alexander Makhlin of Kinea Design LLC, who collaborated in the design of the robot and built it. This work was supported by NSF grant IOB-0517683 to MAM and by an NSF grant CMMI-0941674 to MAM, NAP and GVL. Partial support was provided by NSF CAREER CTS-0134546 to NAP and CBET-0828749 to NAP and MAM.

References

[1] Curet O M, Patankar N A, Lauder G V and MacIver M A 2010 Aquatic manoeuvering with counter-propagating waves: a novel locomotive strategy *J. R. Soc. Interface* at press (doi:10.1098/rsif.2010.0493)

[2] MacIver M A, Sharabash N M and Nelson M E 2001 Prey-capture behavior in gymnotid electric fish: motion analysis and effects of water conductivity *J. Exp. Biol.* **204** 543–57

[3] Snyder J B, Nelson M E, Burdick J W and MacIver M A 2007 Omnidirectional sensory and motor volumes in an electric fish *PLoS Biol.* **5** 2671–83

[4] MacIver M A, Patankar N A and Shirgaonkar A A 2010 Energy-information trade offs between movement and sensing *PLoS Comput. Biol.* **6** e1000769

[5] Cowan N J and Fortune E S 2007 The critical role of locomotion dynamics in decoding sensory systems *J. Neurosci.* **27** 1123–8

[6] Shirgaonkar A A, Curet O M, Patankar N A and MacIver M A 2008 The hydrodynamics of ribbon-fin propulsion during impulsive motion *J. Exp. Biol.* **211** 3490–503

[7] Blake R W 1983 Swimming in the electric eels and knifefishes *Can. J. Zool.* **61** 1432–41

[8] Childress S 1981 *Mechanics of Swimming and Flying* (Cambridge: Cambridge University Press)

[9] Lighthill J 1969 Hydromechanics of aquatic animal propulsion *Ann. Rev. Fluid Mech.* **1** 413–46

[10] Blake R W 1978 On balistiform locomotion *J. Mar. Biol. Assoc.* **58** 73–80

[11] Lighthill J and Blake R 1990 Biofluid dynamics of balistiform and gymnotiform locomotion: 1. Biological background, and analysis by elongated-body theory *J. Fluid Mech.* **212** 183–207

[12] Epstein M, Colgate J E and MacIver M A 2006 Generating thrust with a biologically-inspired robotic ribbon fin *Proc. 2006 IEEE/RSJ Int. Conf. on Intelligent Robots and Systems, Workshop on Robotic Fish (Beijing, China, 9–15 October 2006)* **1–12** 2412–7

[13] Low K H and Willy A 2006 Biomimetic motion planning of an undulating robotic fish fin *J. Vib. Control* **12** 1337–59

[14] Lauder G V and Tytell E D 2006 Hydrodynamics of undulatory propulsion *Fish Biomechanics* (*Fish Physiology*

vol 23) ed R E Shadwick and G V Lauder (San Diego, CA: Elsevier) pp 425–68
[15] Barrett D S, Triantafyllou M S, Yue D K P, Grosenbaugh M A and Wolfgang M J 1999 Drag reduction in fish-like locomotion *J. Fluid Mech.* **392** 183–212
[16] Kato N 2000 Control performance in the horizontal plane of a fish robot with mechanical pectoral fins *IEEE J. Ocean. Eng.* **25** 121–9
[17] Bandyopadhyay P R 2002 Maneuvering dynamics of fish and small underwater vehicles *Integr. Comp. Biol.* **42** 102–17
[18] Long J H J, Koob T J, Irving K, Combie K, Engel V, Livingston N, Lammert A and Schumacher J 2006 Biomimetic evolutionary analysis: testing the adaptive value of vertebrate tail stiffness in autonomous swimming robots *J. Exp. Biol.* **209** 4732–46
[19] Lauder G V, Anderson E J, Tangorra J and Madden P G A 2007 Fish biorobotics: kinematics and hydrodynamics of self-propulsion *J. Exp. Biol.* **210** 2767–80
[20] Hultmark M N, Leftwich M and Smits A J 2007 Flowfield measurements in the wake of a robotic lamprey *Exp. Fluids* **43** 683–90
[21] Triantafyllou M S and Triantafyllou G S 1995 An efficient swimming machine *Sci. Am.* **272** 64–70
[22] Lauder G V and Madden P G A 2006 Learning from fish: kinematics and experimental hydrodynamics for roboticists *Int. J. Autom. Comput.* **4** 325–35
[23] Shirgaonkar A A, MacIver M A and Patankar N A 2011 The balance between drag and thrust in undulatory propulsion (in preparation)
[24] Gray J and Lissmann H W 1964 The locomotion of nematodes *J. Exp. Biol.* **41** 135–54
[25] Maladen R, Ding Y, Li C and Goldman D 2009 Undulatory swimming in sand: subsurface locomotion of the sandfish lizard *Science* **325** 314
[26] Gillis G B 1998 Environmental effects on undulatory locomotion in the American eel Anguilla rostrata: kinematics in water and on land *J. Exp. Biol.* **201** 949–61
[27] Torres R R, Curet O M, Lauder G V and MacIver M A 2011 The kinematics of ribbon fin propulsion in a weakly electric knifefish (in preparation)
[28] MacIver M A, Pantakar N A, Lauder G V, Shirgaonkar A A and Curet O M 2011 Why knifefish are shaped like knives *Proc. R. Soc.* B (submitted)
[29] Munson B R, Young D F and Okiishi T H 2002 *Fundamentals of Fluid Mechanics* 4th edn (New York: Wiley)